



Boosting visible light conversion in the confined pore space of nanoporous carbons



Alicia Gomis-Berenguer ^a, Jesus Iniesta ^b, Artur Moro ^c, Valter Maurino ^d, Joao C. Lima ^c, Conchi O. Ania ^{a,*}

^a Instituto Nacional del Carbon (INCAR,CSIC), Apdo. 73, 33080 Oviedo, Spain

^b Institute of Electrochemistry, Faculty of Science, Univ. Alicante, 03080, Spain

^c Dpt. Chemistry, REQUIMTE/CQFB, Faculdade de Ciências e Tecnologia, Universidade Nova de Lisboa, 2829-516 Lisboa, Portugal

^d Department of Chimica, Università di Torino, Via P. Giuria 5-7, 10125 Torino, Italy

ARTICLE INFO

Article history:

Received 8 May 2015

Received in revised form

9 September 2015

Accepted 10 September 2015

Available online 14 September 2015

ABSTRACT

We showed the effect of commensurate confinement in the pores of nanoporous carbons in the conversion of visible light into a chemical reaction. By using a series of nanoporous carbons with a controlled distribution of pore sizes obtained from a gradual activation under moderate conditions, we have demonstrated the superior conversion of light in the constrained pore space of the carbons compared to values in solution. Besides a more efficient conversion of light, nanopore confinement resulted in a 100–200 nm redshift in the wavelength onset of the photochemical reaction. The visible light activity was boosted in pores which sizes match the dimensions of the confined compound. We attribute this to the enhanced splitting and charge separation of the photogenerated species in the nanopores, due to the proximity of the charge carriers and the adsorbed molecules.

© 2015 Elsevier Ltd. All rights reserved.

1. Introduction

Our recent research has put forward the intrinsic photochemical activity of nanoporous carbons under adequate illumination conditions [1,2], demonstrating their ability to photogenerate radical oxygen species (ROS) in aqueous environments [3,4]. This has opened new perspectives in the field of applied photochemistry based on carbon materials covering from photooxidation reactions for environmental remediation and photoassisted regeneration of exhausted carbon adsorbents [5,6] to water splitting [7], enhanced adsorption/oxidation or photoluminescence [8–11]. Despite the rising interest in the field, there is still a multitude of fundamental questions that are worth investigating to exploit the potentialities of light-responsive carbons for technological applications related to the conversion of light into chemical reactions. In this regard, several authors have reported the possibility to modulate the light absorption features of

nanoporous carbons upon surface functionalization, favoring the conversion of low energy photons from the visible light spectrum into chemical reactions (i.e., photoelectrochemical water splitting) by introducing N and S-containing surface groups on the carbon matrix [7,11–14].

Aiming at throwing some light on the field, we herein show the dependence of the photochemical response of carbons with the nanopore confinement and the wavelength of the irradiation source, choosing the photooxidation of phenol as a model reaction. Conceptually, the confinement of light in constrained pore spaces has been reported to enhance light–matter interactions, allowing for instance measurements of low quantum yield photochemical reactions [15,16]. Some studies have been performed on the accommodation of photoactive guests inside the internal voids or nanocages of porous hosts (mostly for zeolites and MOFs), but yet little is known about the effects of exciton confinement in the pore structure of light-responsive carbons where the porous host exhibits strong absorption features. From a technological viewpoint, only the understanding of the fundamentals of the photochemistry of nanoporous carbons would allow a successful integration of these photoassisted reactions to a wide panel of technological processes in the near future.

* Corresponding author.

E-mail address: conchi.ania@incarcscic.es (C.O. Ania).

2. Experimental

2.1. Materials synthesis

A series of nanoporous carbons with progressively changing pore structures were obtained from activation of coal under CO₂ atmosphere (10 °C/min up to 850 °C in 100 mL/min N₂, then switch to CO₂, 10 mL/min) for variable periods of time. The samples were labeled as F1 and F4, where the number represents the increasing burn-off degree achieved in the activation. Selected physicochemical characteristics along with the main textural parameters for porosity characterization of the samples are compiled in Table 1.

2.2. Irradiation set-up and phenol photooxidation

A Xe lamp (300 W) coupled to a monochromator was used to irradiate the samples. The photon flux arriving at each wavelength was measured by ferrioxalate actinometry [19], and used to normalize the photochemical conversions (see Fig. S1 in the Electronic Supplementary Information File, ESI). Before irradiation, suspensions of the carbons in a phenol solution are allowed to equilibrate until all phenol is completely adsorbed; then they are irradiated for 30 min under stirring. The solution is filtered out and analyzed by reverse phase HPLC and UV–visible spectrophotometry. The carbons are further extracted with ethanol and the alcoholic solution is also analyzed to identify reaction intermediates. Extraction yields are previously determined for each pure compound and carbon. The corresponding blanks of direct degradation upon irradiation in the absence of catalyst were carried out under similar conditions. All the measurements were done at least in triplicates; average values and standard deviations are presented.

2.3. Characterization techniques

The textural properties of the samples were determined by means of N₂ and CO₂ adsorption at –196 and 0 °C, respectively, in volumetric analyzers. Before the experiments, the samples were outgassed at 120 °C overnight to constant vacuum (10^{–4} Torr). The specific surface area, S_{BET}, and pore volumes were evaluated from

Table 1
Main physicochemical characteristics of the studied nanoporous carbons obtained from gas adsorption, chemical composition (wt.%), and surface pH.

	F	F1	F4
S _{BET} [m ² g ^{–1}]	799	1145	1800
V _{PORES} [cm ³ g ^{–1}] ^a	0.35	0.5	0.84
V _{MICROPORES} [cm ³ g ^{–1}] ^b	0.31	0.45	0.04
V _{MESOPORES} [cm ³ g ^{–1}] ^b	0.03	0.04	0.15
W _o N ₂ [cm ³ g ^{–1}] ^c	0.34	0.55	0.80
W _o CO ₂ [cm ³ g ^{–1}] ^c	0.25	0.33	0.36
L [nm] ^d	0.56	0.68	0.77
Porosity, e [%] ^e	38	45	54
C (wt.%)	96.15	95.92	95.85
H (wt.%)	0.70	0.45	0.22
N (wt.%)	0.14	0.11	0.09
O (wt.%)	2.90	3.43	3.73
Surface pH	8.1	8.2	8.0

^a Total pore volume evaluated from the N₂ adsorption isotherms at –196 °C at relative pressure of 0.99.

^b Pore volume evaluated from the N₂ adsorption isotherms at –196 °C using the 2D-NLDFT-HS method [17].

^c Pore volume evaluated from the Dubinin-Radushkevich method applied to both CO₂ and N₂ adsorption isotherms.

^d Mean narrow micropore size evaluated from the Stoeckli-Ballerini equation applied to the CO₂ adsorption isotherms.

^e Porosity (%) evaluated from the bulk and helium densities [18]
e (%) = [1 – (ρ_{apparent}/ρ_{Helium})] × 100.

the gas adsorption isotherms. The pore size distribution in the full micropore range was calculated using the 2D-NLDFT-HS model assuming surface heterogeneity of carbon pores [17]. The mean narrow micropore size was evaluated from the Stoeckli-Ballerini equation applied to the CO₂ adsorption isotherms [18]. The carbon materials were further characterized by elemental analysis (LECO CHNS-932 and VTF-900 automatic analyzers) and surface pH [20]. X-ray photoelectron spectra were recorded on a SPECS spectrometer with a Phoibos 100 hemispherical analyzer with a multichannel detector. The base pressure in the ultra high vacuum chamber was below 10^{–7} kPa. The X-ray radiation source was monochromatic AlKα (1486.74 eV) at 100 W X-ray power and anode voltage of 14 kV. The photo-excited electrons were analyzed in constant pass energy mode, using pass energy of 50 eV for the Surrey spectra and 10 eV for the high resolution core level spectra. During data processing of the XPS spectra, binding energy values were referenced to the C 1s peak at 284.6 eV. The CasaXPS software package was used for acquisition and data analysis. A Shirley-type background was subtracted from the signals. Recorded spectra were always fitted using Gauss–Lorentz curves, in order to determine the binding energy of the different element core levels more accurately. The error in binding energy was estimated to be ca. 0.1 eV. Raman spectroscopy was performed by excitation with green laser light (532 nm) in the range between 800 and 3550 cm^{–1}. The spectra were acquired in a Jobin-Yvon Horiba HR800 spectrometer equipped with a Leica microscope. The acquisition time for each spectrum was 300 s; to guarantee a representative sampling, spectra were recorded in 4 different spots for each sample.

2.4. Spin trapping electron spin resonance (ESR) measurements

The formation of paramagnetic species in solution during irradiation of the carbon suspensions was detected by a nitron spin trapping agent (5,5-dimethylpyrrolone-N-oxide, DMPO). This compound is capable of forming spin adducts with hydroxyl and superoxide radicals, creating more stable nitron radicals that are easily detected by ESR spectroscopy in aqueous solution. About 0.5 g/L of the carbon samples were suspended in 5 ml of HClO₄ buffer (pH 3), and the appropriate volume of DMPO was added to the suspension to reach a final concentration of 18 mM. Samples were introduced in capillary quartz tubes and irradiated for 5, 10, 20 and 60 min (Philips TL K40 W/05 lamp, with a broad emission peak centered at 365 nm). ESR spectra were immediately recorded from the solution (after filtering out the solids) at room temperature on a Bruker ESP 300E X band spectrometer with the following spectral parameters: receiver gain 105; modulation amplitude 0.52 G; modulation frequency 100 KHz, microwave frequency 9.69 GHz; microwave power 5.024 mW; conversion time 40.96 ms; center field 3450 G, sweep width 120 G.

3. Results and discussion

To tackle the study of the carbon/light interactions occurring inside nanoconfined pore spaces it becomes crucial to avoid other secondary reactions inherent to high energy irradiation sources and porous materials (i.e. direct photolysis and adsorption). We have developed a strategy to overcome this limitation based on evaluating the efficiency of a photochemical reaction –for instance, the photooxidation of phenol in solution–occurring in the inner void space of nanoporous materials (see Scheme in ESI). The approach consists in introducing the target compound inside the pore structure of the nanoporous carbon (adsorbed), and illuminating the suspension in water for a predetermined time. After irradiation, both components of the suspension (solution and

carbon) are analyzed to determine if there has been lixiviation to the solution (not being the case for any of the studied materials) and the compounds still retained inside the porosity of the carbon after light exposure, using extraction in ethanol. This allows to determine the extent of the photochemical reaction that takes place inside the porosity of the material [1,2].

The starting carbon (sample F) of this study is a biomass-derived material, chosen for its photochemical activity under UV light [2] and narrow distribution of pore sizes within the micropore range as evidenced from gas adsorption data obtained from nitrogen and carbon dioxide (Fig. 1, Table 1). To gain additional insight on the effect of light conversion inside nanoconfined pore spaces, sample F was activated under CO₂ atmosphere for variable periods of time to obtain samples F1 and F4 with increasing burn-off degrees. It is important to highlight that during the activation reaction the chemical composition of the carbons remained almost unaltered (Table 1), with changes exclusively seen in the pore volume, surface area and particularly the narrow microporosity. This was further confirmed by additional characterization of the samples by XPS (see discussion below) and TPD-MS (Fig. S2).

Fig. 1 shows the effect of the activation under strict controlled conditions on the narrow microporosity of the carbons by the analysis of the carbon dioxide adsorption isotherms [21]. The isotherm of the pristine carbon F displays a concave shape characteristic of materials with a well-defined narrow microporosity; the curvature at low relative pressures becomes less pronounced with the burn-off degree, whereas at higher relative pressures the isotherms intersect each other, with the activated samples displaying larger gas uptakes. This confirms the enlargement of the micropores with the activation treatment, also evidenced by the L parameter representing the mean pore size (Table 1) and the distribution of pore sizes in the full micro-mesopore range (Fig. 1).

For the photochemical experiments, the carbons were loaded with a fixed amount of phenol per unit mass (ca. 0.09 mmol/g), chosen to keep the loading of phenol below the saturation limit for all three studied carbons (Fig. S3). This procedure allows confining the adsorbed fraction of phenol into the narrow microporosity of the carbons [22,23]. This avoids desorption in the course of the irradiation (thus contribution of photolytic breakdown is discarded) [1,2]. It also leads to high photoconversion values, thereby minimizing any experimental error associated to the quantification of the compounds in the extracts. The wavelength dependence of

the photochemical activity of the carbons was determined using monochromatic light. Unlike most studies dealing with polychromatic light, this allows discriminating between the contributions of the high/low energy photons, and hence isolating any actual visible-light conversion without biased interpretations.

Fig. 2 shows phenol conversion values (data from the extracts) upon irradiation of the pre-loaded nanoporous carbons at selected wavelengths. As the incident photon flux is different for each wavelength (Fig. S1), conversion was normalized per photon flux to allow direct comparison of all data. For clarity, the measured (non-corrected) values of phenol conversion at each wavelength are also presented in Fig. 2C.

The composition of the extracts after irradiation of the pre-loaded carbons confirmed the photoinduced degradation of phenol in the constrained pore space for all the studied samples and at all selected wavelengths. This is most remarkable considering that carbons are strong light absorbers, and hence a large fraction of the light is not expected to reach the adsorbed molecules retained in the inner porosity. Most importantly, phenol conversion in the confined state is higher than that of direct photolysis from solution (ca. below 2%) as seen in Fig. 2C, corroborating the outstanding role of nanoconfinement in enhancing the light conversion into a chemical reaction. Also, whereas direct photochemical breakdown of phenol from solution is negligible at wavelengths above 300 nm, high conversion values are obtained at 450 and 500 nm when the photochemical reaction was carried out inside the confined pore space. This corresponds to over 100–200 nm redshift in the wavelength onset for the photochemical reaction compared to photolysis in solution, and clearly demonstrates the ability of nanoporous carbons to convert sunlight into a chemical reaction.

Interestingly, the photochemical performance followed a U-shaped pattern rather than a decreasing trend with the wavelength (Fig. 2A). All three carbons showed a minimum at 400 nm, derived from very low conversion values (Fig. 2C), whereas at wavelengths corresponding to visible light (i.e., 450 and 500 nm), the conversion rose again with values very close to those obtained at 269 nm. In our previous studies we also observed low conversion values at 400 nm using a different lamp set-up, and tentatively attributed this to the low photon flux provided by the source at this wavelength, rather than to the inactivity of the carbon materials [1]. This hypothesis however would not apply to these systems since the incident photon flux at 400 nm is several times higher than those

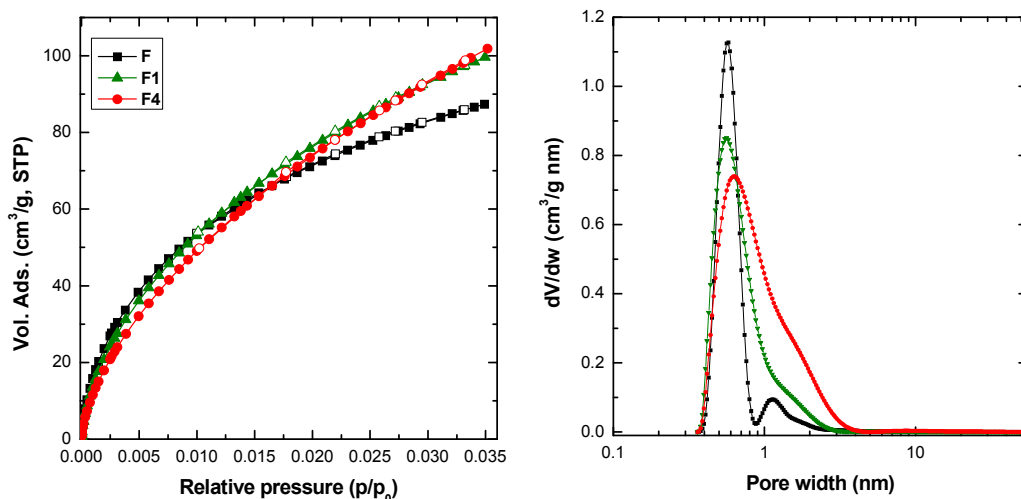


Fig. 1. (left) Carbon dioxide adsorption isotherms measured at 0 °C showing the differences in the narrow microporosity of the studied carbons. (right) Pore size distributions obtained from the 2D-NLDFT-HS model applied to the N₂ adsorption isotherms at –196 °C. (A colour version of this figure can be viewed online.)

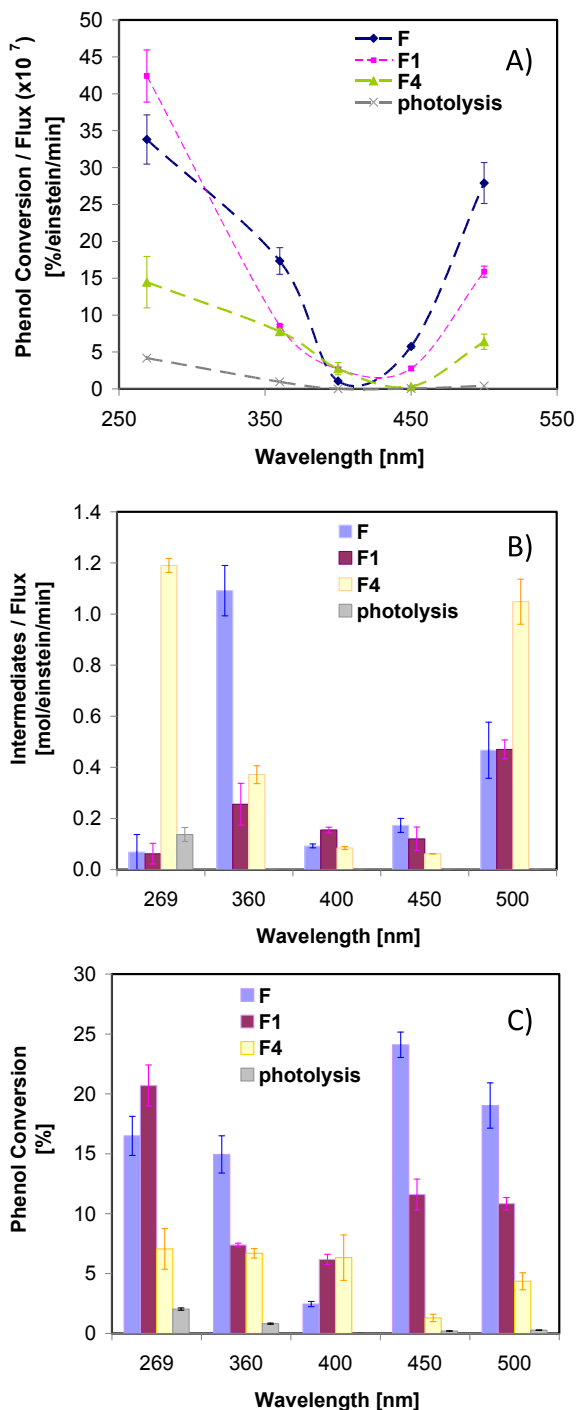


Fig. 2. A) Phenol conversion and B) amount of degradation intermediates (dihydroxylated benzenes) per incident flux at different wavelengths on all three studied carbons; C) actual (non-corrected) phenol conversion values at each wavelength. (A colour version of this figure can be viewed online.)

measured for the rest of the wavelengths (Fig. S1). Yet the conversion values at 400 nm are much lower than those of the other wavelengths in the series.

Interesting features are revealed for the wavelength dependence of the photooxidation yields with the activation treatment. Despite all three carbons showed a similar wavelength onset of the photochemical activity -in agreement with the performance described for other nanoporous carbons in our earlier works- [1], we herein report the correlation of these differences in conversion

with the confinement state of the adsorbed molecules. Phenol conversions (Fig. 2) followed the general trend: $F > F1 > F4$, with larger differences at higher energy photons (lower wavelengths), demonstrating a more successful exploitation of light in tight confinements. Only the performance at 269 nm slightly escapes from this trend, as the photochemical conversion inside F and F1 is rather alike. The amount of degradation intermediates (dihydroxylated benzenes) also varies with the confinement and the illumination conditions (Fig. 2B). At 269 nm both phenol and its aromatic intermediates are efficiently decomposed, whereas as the irradiation becomes less energetic the amount of intermediates gradually increases -conversion of phenol does not follow the same trend-; this points out that the photooxidation reaction is hindered or delayed to some extent, likely due to the difficulty in pursuing the oxidation of dihydroxylated compounds under visible light.

The dependence of the yield of the photochemical reaction with the average pore size at different wavelengths is more clearly seen in Fig. 3. As a general trend, the photochemical conversion of phenol gradually decreased with the enlargement of the average micropore size, being the effect less remarkable at large wavelengths. Data also showed a wavelength dependent threshold pore size for an optimum exploitation of the light. At 269 nm the conversion of light was enhanced for pores below 0.7 nm (with small differences between them) whereas the photochemical response was drastically reduced when the pores were widened by 0.1 nm. For higher wavelengths, the drop in the photochemical conversion is very pronounced, particularly at 500 nm where the performance is

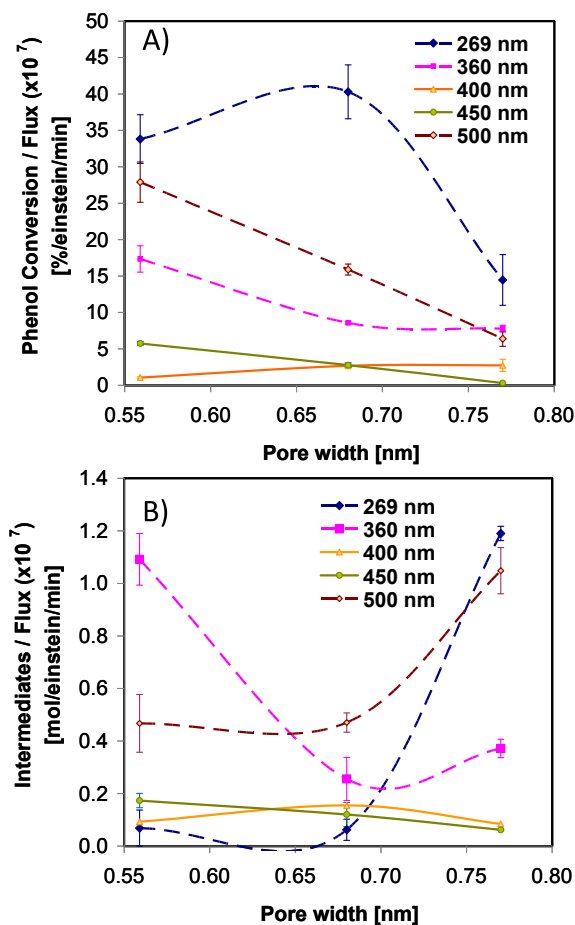


Fig. 3. Correlation of normalized phenol photooxidation conversion (A) and intermediates detected (B) with the mean micropore size at different wavelengths. (A colour version of this figure can be viewed online.)

quite close to that at 269 nm for pore apertures of 0.56 nm.

To understand this behavior we must consider the confinement state of the adsorbed molecules in the constrained pore space. As mentioned above, the amount of phenol incorporated in the pores was below the saturation limit of the carbons to restrict the confinement of the adsorbed molecules to the narrow microporosity (molecular dimensions of phenol are $0.80 \times 0.67 \times 0.15$ nm) [24] in single adsorption layers (maximizing host–guest interactions). According to literature [22,23], adsorption of phenol and its derivatives on hydrophobic carbons is governed by dispersive interactions with molecules predominantly adsorbed in an edge-wide orientation, with the aromatic ring parallel to the pore walls (plane-on) and the hydroxyl moiety projecting away from pore walls towards the aqueous phase [25].

On the other hand, the light absorption features of amorphous carbons depend on the Density Of electronic States, DOS, (mainly sp^2/sp^3 hybridization ratio of the carbon atoms), and in the UV range are dominated by $\pi-\pi^*$ and $\sigma-\pi^*$ transitions involving free zig-zag sites and carbene-like sites [23–28]. Under sunlight irradiation, some other transitions involving the activation of chromophoric groups on the carbon surface have been proposed [7–9,29]. Considering the low and quite similar functionalization of these carbons (Table 1), we expect the latter contribution to be small.

Hence, irradiation of the carbons gives rise to the formation of excitons (holes or electrons), which when splitting is favored can participate in charge transfer reactions with electron donors present in the reaction medium [30,31]. The superior conversion of the carbons compared to the photolytic reaction confirms that the light conversion is boosted in the constrained pore space, and the differences for the three materials point out the role of confinement.

Regarding the nature of excitons, and considering the low (and similar) functionalization and polarity of these carbons and their electronic properties (dielectric constants of nanoporous carbons are lower than those of n-type semiconductors as TiO_2 and higher than those of other carbon nanostructures with higher conductivity such as carbon blacks, graphene or fullerenes) [32,33], medium to low range (Frenkel-like) exciton structures originated from the sp^2 carbon clusters are expected to be dominant, while the contribution of charge-transfer excitons formed by localized states involving both O and C atoms is expected to be small. This is consistent with the behavior reported for other carbons nanostructures based on experimental observations and molecular simulations [34,35].

In this regard, Raman spectra of the three studied carbons show similar profiles for all of them, with the characteristic D and G bands broad of disordered carbons in the region between 1000 and 2000 cm^{-1} (Fig. S4). The structural ordering of the carbon network was evaluated by the I_G/I_D ratio upon deconvolution of the spectra (Table 2); increasing the burn-off degree caused a slight increase in the I_G/I_D ratio, although changes are subtle. The broadening of the D band is also similar -indicating similar sizes of graphitic crystallite domains-, and overall the three carbons display similar structural disorder. Furthermore, the three carbons also display similar electrical conductivity values (ca. $0.5\text{--}0.8\text{ S/cm}$).

Considering all the above, the characterization of the carbons confirmed that the smooth CO_2 activation treatment affected

mostly the enlargement of the micropores (Fig. 1). Indeed, no significant changes were detected either on the surface functionalization of the activated samples (Table 1), on the disorder degree derived from the removal of carbon atoms at the edges (Table 2), or by inducing structural defects due to modifications in the sp^2/sp^3 hybridization of carbon atoms (Fig. 4). All of these would eventually have a strong effect in the optical characteristics (ca. creation of distorted sites in the DOS) of the carbons, and the stabilization of the photogenerated carriers through the delocalization within the conjugated sp^2 network of the basal planes. On the contrary, differences must be attributed to the fate of the charge carriers in the constrained pore space. The tight confinement of phenol molecules in pores that commensurate the molecular size facilitates the exciton splitting through the reaction with electron donors, boosting the conversion of light. Several scenarios might be plausible; the first one is that the holes might directly react with the adsorbed phenol molecules, as the on-plane orientation favors the proximity of the π electrons of the aromatic ring towards the pore walls where the exciton is generated (however we do not have direct evidence for this).

Another possibility is the stabilization of the holes through the oxidation of water molecules co-confined in the pores along with phenol to form hydroxyl radicals. This is supported by the detection of ROS after irradiation of aqueous suspensions of the carbons using spin resonance spectroscopy and nitrones as spin trapping chemicals (Fig. 5). The photogeneration of hydroxyl radicals for all the carbons corroborates the separation of the exciton and migration to the aqueous solution. When phenol is introduced inside the nanopores, the radicals are more efficiently used for the photooxidation of the adsorbed molecules, as corroborated by the nature of the intermediates detected (namely dihydroxylated benzenes).

4. Conclusions

We report the superior conversion of light into a chemical reaction boosted in the constrained pore space of nanoporous carbons. Matching of the molecular dimensions of the target compound confined in the carbon pore network results in a 100 nm red-shift of light conversion. As a result, the proximity between the photogenerated charge carriers and the adsorbed molecule in the constrained pore space facilitates the exciton splitting and the charge separation, enhancing the conversion of the photooxidation reaction under both UV and sunlight.

We anticipate that tuning the porous network of nanoporous carbons with photochemical activity opens up an interesting strategy to master the conversion of light in chemical reactions, especially favoring the utilization of sunlight. The control of the pore structure of nanoporous carbons is no longer a challenge, which offers an interesting opportunity to improve light harvesting through the control of the physicochemical features of low cost porous carbons to facilitate exciton splitting.

Owing to the recently gained interest on the use of carbon materials in photochemical applications and their versatility of forms, structures and precursors, our findings demonstrate that it is highly feasible to push the use of nanoporous carbons as sustainable metal-free and low cost photoactive materials, particularly when much attention is lately being paid to the investigation of more sophisticated forms of carbons (graphene, nanotubes, graphite oxide), so far considered non photoactive under visible light.

The challenge still remains in the further enhancement of the photochemical activity by balancing the surface composition, porosity, and charge-carrier mobility. The dependence of the photochemical activity of the studied carbons with the nanopore confinement described here is expected to be valuable in general

Table 2
Raman shift and width values for the D and G bands calculated from the deconvoluted spectra.

	D shift (cm^{-1})	G shift (cm^{-1})	D band FWHM	G band FWHM	I_G/I_D
F	1343	1586	126	73	1.03
F1	1342	1593	122	64	0.96
F4	1338	1591	114	64	0.86

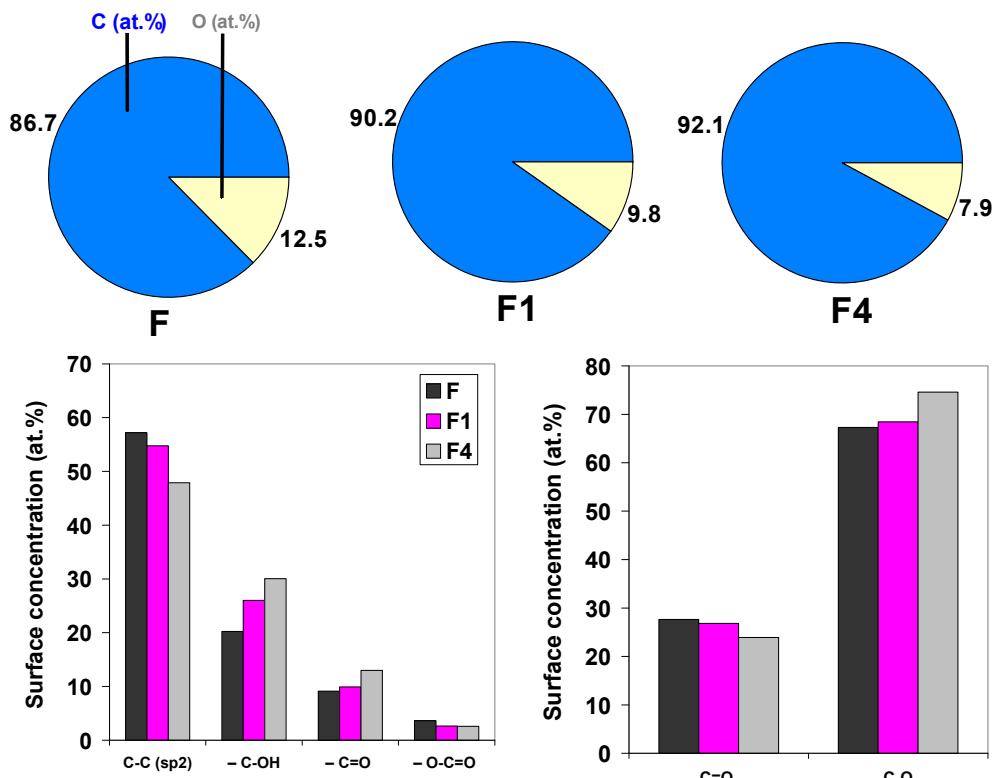


Fig. 4. Surface concentration (atomic %) of heteroatoms (top) and distribution of carbon and oxygen species (down) obtained by fitting the C 1s and O 1s core level peaks of XPS spectra. (A colour version of this figure can be viewed online.)

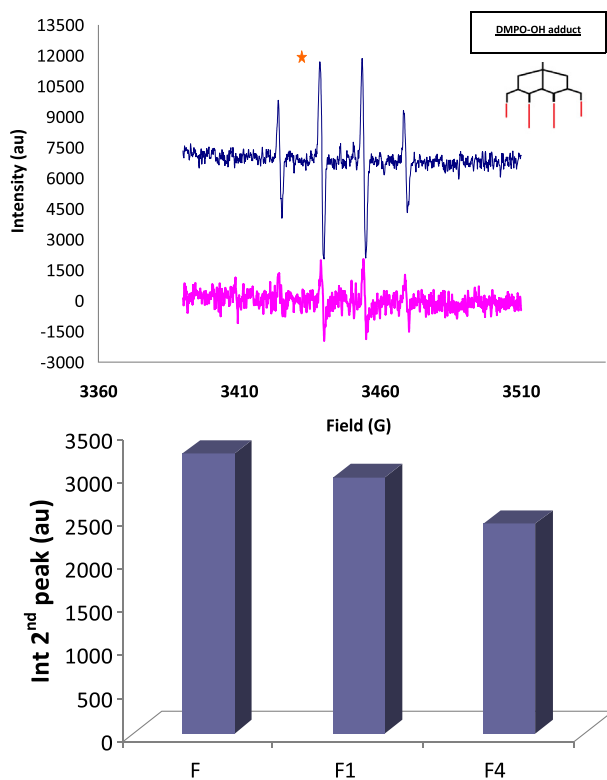


Fig. 5. (top) Characteristic ESR signal of DMPO-OH adduct obtained upon 20 min of irradiation of aqueous suspensions of a nanoporous carbon and titania powders for comparison. (down) Quantification of the radical species detected from the signal corresponding to DMPO-OH adducts by integration of the second peak in the 1:2:2:1 quartet profile (marked as *). (A colour version of this figure can be viewed online.)

for targeting other applications in the fields of solar energy conversion (e.g. water splitting, carbon photofixation reactions, photovoltaic devices) on light responsive carbons.

Acknowledgments

COA thanks the financial support of MINECO (CTM2014-56770-R). AGB thanks MINECO for her PhD fellowship (BES-2012-060410).

Appendix A. Supplementary data

Supplementary data related to this article can be found at <http://dx.doi.org/10.1016/j.carbon.2015.09.047>.

References

- [1] L.F. Velasco, J.C. Lima, C.O. Ania, Visible-light photochemical activity of nanoporous carbons under monochromatic light, *Angew. Chem. Int. Ed.* 53 (2014) 4146–4148.
- [2] L.F. Velasco, J.B. Parra, I.M. Fonseca, J.C. Lima, C.O. Ania, Photochemical behaviour of activated carbons under UV irradiation, *Carbon* 50 (2012) 249–258.
- [3] L.F. Velasco, V. Maurino, E. Laurenti, I.M. Fonseca, J.C. Lima, C.O. Ania, Photo-induced reactions occurring on activated carbons. A combined photooxidation and ESR study, *Appl. Catal. A General* 452 (2013) 1–8.
- [4] L.F. Velasco, V. Maurino, E. Laurenti, C.O. Ania, Light-induced generation of radicals on semiconductor-free carbon photocatalysts, *Appl. Catal. A General* 453 (2013) 310–315.
- [5] L.F. Velasco, R.J. Carmona, J. Matos, C.O. Ania, Performance of activated carbons in consecutive phenol photooxidation cycles, *Carbon* 73 (2014) 206–215.
- [6] I. Velo-Gala, J.J. Lopez-Peñalver, M. Sanchez-Polo, J. Ribera-Utrilla, Activated carbon as photocatalyst of reactions in aqueous phase, *Appl. Catal. B* 142 (2013) 694–704.
- [7] C.O. Ania, M. Seredych, E. Rodriguez-Castellon, T.J. Bandoz, Visible light driven photoelectrochemical water splitting on metal free nanoporous carbon promoted by chromophoric functional groups, *Carbon* 79 (2014) 432–441.
- [8] L. Bao, Z.L. Zhang, Z.Q. Tian, L. Zhang, C. Liu, Y. Lin, B. Qi, D.W. Pang,

- Electrochemical tuning of luminescent carbon nanodots: From preparation to luminescence mechanism, *Adv. Mater* 23 (2011) 5801–5806.
- [9] Q. Bao, J. Zhang, C. Pan, J. Li, C.M. Li, J. Zang, D.Y. Tang, Recoverable photoluminescence of flame-synthesized multiwalled carbon nanotubes and its intensity enhancement at 240K, *J. Phys. Chem. C* 111 (2007) 10347–10352.
- [10] T.J. Bandoz, E. Rodriguez-Castellon, J.M. Montenegro, M. Seredych, Photoluminescence of nanoporous carbons: opening a new application route for old materials, *Carbon* 77 (2014) 651–659.
- [11] M. Seredych, L. Messali, T.J. Bandoz, Analysis of factors affecting visible and UV enhanced oxidation of dibenzothiophenes on sulphur-doped activated carbons, *Carbon* 62 (2013) 356–364.
- [12] D. Pan, J. Zhang, Z. Li, M. Wu, Hydrothermal route for cutting graphene sheets into blue-luminescent graphene quantum dots, *Adv. Mater* 22 (2010) 734–738.
- [13] T.J. Bandoz, J. Matos, M. Seredych, M.S.Z. Islam, R. Alfano, Photoactivity of S-doped nanoporous activated carbons: a new perspective for harvesting solar energy on carbon-based semiconductors, *Appl. Catal. A* 445 (2012) 159–165.
- [14] M. Seredych, T.J. Bandoz, Effect of the graphene phase presence in nanoporous S-doped carbon on photoactivity in UV and visible light, *Appl. Catal. B* 147 (2014) 842–850.
- [15] B. Li, F. Li, S. Bai, Z. Wang, L. Sun, Q. Yang, C. Li, Oxygen evolution from water oxidation on molecular catalysts confined in the nanocages of mesoporous silicas, *Energy Environ. Sci.* 5 (2012) 8229–8233.
- [16] A. Corma, H. Garcia, Zeolite-based photocatalysts, *Chem. Comm.* (2004) 1443–1459.
- [17] J. Jagiello, J.P. Olivier, Carbon slit pore model incorporating surface energetical heterogeneity and geometrical corrugation, *Adsorption* 19 (2013) 777–783.
- [18] F. Rouquerol, J. Rouquerol, K.S.W. Sing, P. Llewellyn, G. Maurin, *Adsorption by Powders, Porous Solids Principles, Methodology, Applications*, second ed., Elsevier, 2014.
- [19] H.J. Kuhn, S.E. Braslavsky, R. Schmidt, Chemical actinometry, *Pure Appl. Chem.* 76 (2004) 2105–2146.
- [20] J.S. Noh, J.A. Schwarz, Estimation of the point of zero charge of simple oxides by mass titration, *J. Colloid Interface Sci.* 130 (1989) 157–164.
- [21] D. Lozano-Castelló, D. Cazorla-Amorós, A. Linares-Solano, Usefulness of CO₂ adsorption at 273K for the characterization of porous carbons, *Carbon* 42 (2004) 1233–1442.
- [22] L.F. Velasco, C.O. Ania, Understanding phenol adsorption mechanisms on activated carbons, *Adsorption* 17 (2011) 247–254.
- [23] L.R. Radovic, C. Moreno-Castilla, J. Rivera-Utrilla, *Chemistry, Physics of Carbon*, Radovic LR, Marcel Dekker, New York, 2000, pp. 227–405.
- [24] K. Nakagawa, A. Namba, S.R. Mukai, H. Tamon, P. Ariyadejwanich, W. Tanthapanichakoon, Adsorption of phenol and reactive dye from aqueous solution on activated carbons derived from solid wastes, *Water Res.* 38 (2004) 1791–1798.
- [25] D.D. Singh, Surface orientation of phenol molecules adsorbed from aqueous solution by carbon-blacks, *Ind. J. Chem.* 9 (1971) 1369.
- [26] A.D. Modestov, J. Gun, O. Lev, Graphite photoelectrochemistry study of glassy carbon, carbon-fiber and carbon-black electrodes in aqueous electrolytes by photocurrent response, *Surf. Sci.* 417 (1998) 311–322.
- [27] J. Robertson, Mechanical properties and coordinations of amorphous carbons, *J. Phys. Rev. Lett.* 68 (1992) 220–223.
- [28] L.R. Radovic, B. Bockrath, On the chemical nature of graphene edges: origin of stability and potential for magnetism in carbon materials, *J. Am. Chem. Soc.* 127 (2005) 5917–5927.
- [29] R. Ocampo-Pérez, M. Sánchez-Polo, J. Rivera-Utrilla, R. Leyva-Ramos, Enhancement of the catalytic activity of TiO₂ by using activated carbon in the photocatalytic degradation of cytarabine, *Appl. Catal. B Environ.* 104 (2011) 177–184.
- [30] Y. Zhao, R. Nakamura, K. Kamiya, S. Nakanishi, K. Hashimoto, Nitrogen-doped carbon nanomaterials as non-metal electrocatalysts for water oxidation, *Nat. Comm.* 4 (2013) 2390.
- [31] D. Jana, C.L. Sun, L.C. Chen, K.H. Chen, Effect of chemical doping of boron and nitrogen on the electronic, optical, and electrochemical properties of carbon nanotubes, *Prog. Mater. Sci.* 58 (2013) 565–635.
- [32] A. Wang, D.D.L. Chung, Dielectric and electrical conduction behavior of carbon paste electrochemical electrodes, with decoupling of carbon, electrolyte and interface contributions, *Carbon* 72 (2014) 135–151.
- [33] A. Wypych, I. Bobowska, M. Tracz, A. Opasinska, S. Kadlubowski, A. Krzywania-Kaliszewska, P. Grobelny, Wojciechowski, Dielectric properties and characterisation of titanium dioxide obtained by different chemistry methods, *J. Nanomater.* 124814 (2014) 1–10.
- [34] D. Lee, J. Seo, X. Zhu, J. Lee, H.-J. Shin, J.M. Cole, T. Shin, J. Lee, H. Lee, H. Su, Quantum confinement-induced tunable exciton states in graphene oxide, *Sci. Rep.* 3 (2013) 2250–2255.
- [35] X. Zhu, H. Su, Exciton characteristics in graphene epoxide, *ACS Nano* 8 (2014) 1284–1289.